Bulletin of Mathematical Biology (2004) **66**, 167–193
doi:10.1016/j.bulm.2003.08.007

A Continuum Model of Motility in Ameboid Cells

MARIA E. GRACHEVA AND HANS G. OTHMER*

Department of Mathematics,
University of Minnesota,
270A Vincent Hall,
Minneapolis, MN 55455,
USA

E-mail: othmer@math.umn.edu

A continuum model of cell motility in ameboid cells based on a viscoelastic description of the cytoplasm and active stress generation controlled by extracellular signals is developed and analyzed. The characteristics of locomotion depend on the specific active stress, elastic and viscous properties of the cytoplasm as well as on the strength of cell–substrate interactions. A one-dimensional version of the model is applied to describe the motion of a fibroblast. The force balance equation for the cell is solved together with reaction diffusion equations describing the dynamics of proteins essential for cell locomotion. The cell deformation is calculated, and the deformation patterns observed experimentally are reproduced by the model. The cell velocity as a function of cell–substrate interaction is also computed for various cell characteristics such as the active stress generated, the cell elasticity and the coupling between cell–substrate interaction and the ability of the cell to contract.

1. INTRODUCTION

Cell motility is an essential process in the development and maintenance of cells, tissues and organs (Chicurel, 2002). During embryonic development cells must translocate to the correct place to form tissues and organs. The immune response to bacterial invasion or infection includes directed movement of white blood cells such as neutrophils and leukocytes to the site of the infection, and wound healing requires movement of epidermal cells such as fibroblasts and keratocytes. However, there can also be a negative side to cell motility in that it is essential for the formation of new capillaries during angiogenesis, and during metastisis of tumor cells. Many other physiological and pathological responses involving cell movement are described in Bray (2001) and Lauffenburger and Horwitz (1996).

There are two major components in the response of ameboid cells to extracellular signals: determination of the direction in which to move, and the movement itself.

*Author to whom correspondence should be addressed.

0092-8240/04/010167 + 27 $30.00/0

Many eukaryotic cells can detect both the magnitude and direction of extracellular signals using receptors embedded in the cell membrane. When the signal is spatially nonuniform they may respond by directed migration either up or down the gradient of the signal, a process called taxis. When the extracellular signal is a diffusible molecule the response is chemotactic, and when it is an adhesion factor attached to the substrate or extracellular matrix (ECM) the process is called haptotaxis (Alberts *et al*., 2002). Movement toward a chemoattractant involves directional sensing and orientation, assembly of the motile machinery, polarization of the cell, and control of the attachment to the substrate or ECM.

Movement of ameboid cells involves at least four different stages: protrusion, attachment to the substrate, translocation of the cell body, and detachment of the rear (Mitchison and Cramer, 1996; Sheetz *et al*., 1999). (1) Cells first extend localized protrusions at the leading edge, which take the form of lamellipodia, filopodia or pseudopodia. Most current models explain force generation at the leading edge by localized actin polymerization and crosslinking (or gelation) of actin filaments. Rho family GTPases are involved in transducing signals from surface receptors to downstream effectors such as the Arp2/3 complex that associate with actin to nucleate filament assembly (Dumontier *et al*., 2000). Behind the protrusion there is a region of actin disassembly, where filaments are disassembled, crosslinks broken and the actin monomers resulting from disassembly freed to diffuse to the site of active polymerization (Alberts *et al*., 2002). In photoactivation experiments with keratocytes it was found that the rate of depolymerization is more-or-less constant throughout the cytoskeleton (Theriot and Mitchison, 1991). (2) Not all protrusions are persistent, in that they must anchor to the substrate or to another cell in order for the remainder of the cell to follow (Soll, 1995). Protrusions are stabilized by formation of adhesive complexes, which serve as sites for molecular signaling and also transmit mechanical force to the substrate. In fibroblasts adhesive complexes are regions of the plasma membrane where integrin receptors, actin filaments, and associated proteins cluster together. These adhesion sites include integrin receptors that bind to the ECM proteins and provide direct cell–substrate connections (Palecek *et al*., 1996; Cox and Huttenlocher, 1998; Zamir and Geiger, 2001). The integrin receptors are confined to the cell plasma membrane, where they diffuse laterally. Integrins located on the ventral surface of the cell associate with substrate ligands and serve as points of cell anchorage, through which force is transmitted to the substrate. Integrins in turn are connected with other supportive proteins that mediate connections with the actin cytoskeleton of the cell. Protein clustering plays a role in creating front/back adhesion asymmetry (Maheshwari *et al*., 2000). During migration the small nascent adhesive complexes (focal complexes) at the front of the cell grow and strengthen into larger, more organized focal adhesions that serve as traction 'pads' over which the cell body moves (Small, 1989). More than fifty proteins have been reported to be associated with focal adhesions or related to ECM adhesions (Zamir and Geiger, 2001). (3) Next, actomyosin filaments contract at the front of the cell and pull the cell body toward the protrusion in fibroblasts,

whereas in other cell types, contraction is at the rear and the cytoplasm is squeezed forward. (4) Finally, cells detach the adhesive contacts at the rear, allowing the tail of the cell to follow the main cell body. In *Dictyostelium discoideum* (Dd) the adhesive contacts are relatively weak and the cells move rapidly ($\sim$20 μm min^{-1}), whereas in fibroblasts they are very strong and cells move slowly. Further details on how these processes produce motion are given elsewhere (Lauffenburger and Horwitz, 1996; Bray, 2001; Boal, 2002).

To achieve directed motion, as opposed to random searching of the environment, either the interactions of a cell with the substrate or the active contractile and protrusive forces generated by the cell must display some asymmetry (Cox and Huttenlocher, 1998). This can result from asymmetric affinity/avidity of the receptors along the cell or/and receptor trafficking. Asymmetries between the front and rear adhesions in fibroblasts have been observed (Munevar *et al*., 2001a), and the patterns of traction forces formed on flexible substrate by motile fibroblast have been studied (Munevar *et al*., 2001b). It was found that the active extensional forces were localized near the leading edge, while the trailing edge served more as a passive anchorage. The mean cell speed exhibits a bell-shaped dependence on the substrate density or ECM ligand concentration, as well as on mean detachment force (Palecek *et al*., 1997). It was also influenced by several other variables related to integrin–ligand interactions, such as ligand level, integrin level and integrin–ligand binding affinities. These factors define the number of cell–substrate bonds, which in turn determines cell–substrate adhesiveness and migration speed (Palecek *et al*., 1997).

Traction force microscopy has recently been used to measure the cell–substrate traction field in normal fibroblasts and in H-ras transformed NIH 3T3 cells (Dembo and Wang, 1999; Munevar *et al*., 2001a,b). It was shown that individual fibroblasts display a complex spatial distribution of traction forces throughout the cell. In normal cells the field of traction forces can be divided into several areas: (i) areas with large traction forces that are located at the cell front and rear, and (ii) an area beneath the nucleus in which the traction forces are small. In this central region traction forces change direction several times, and these sub-regions are separated by bands of high shear. The authors conclude that the anterior region and remainder of the cell are two mechanically-distinct domains (Munevar *et al*., 2001b). The average cell velocity of a normal cell was $\sim$0.19 μm min^{-1}.

The amount of force that a cell exerts also depends on the substrate: on a rigid, adhesive substrate a cell can generate large contractile forces transmitted through actin bundles and adhesion complexes, but on a more pliable substrate it exhibits a less-organized actin network and smaller, weaker adhesion complexes (Lo *et al*., 2000). Since we ultimately want to describe how a cell interacts with a substrate, we concentrate our attention here on a feedback between cell–substrate interaction and cytoskeleton, specifically cytoskeleton contractile ability due to actin–myosin meshwork contraction and active force generation. There is also a connection between integrins, which mediate the connection between the cell membrane and

the ECM, with actin stress fiber formation and contractility through *Rho* and *Pak* (Defilippi *et al*., 1999; Kaverina *et al*., 2002). Also, an important experimental observation has been made recently (Chew *et al*., 2002), that pointed to the exact location of activation of myosin II motors in motile cells. The experiments were done with the help of a novel biosensor allowing determination of local activity of myosin light chain kinase (MLCK) in motile cells. It has been already established that MLCK enzyme activates myosin II causing it to generate force. It was found (Chew *et al*., 2002) that MLCK is highly active in the lamella of migrating cells, but not in the retracting tail. Transient recruitment of diffuse MLCK to stress fibers before activation was observed. It was concluded that MLCK mediate myosin contractility in the lamella that serves as a driving force for migration. It is also known MLCK activation is indirectly influenced by focal adhesion formation (Martin *et al*., 2002).

The cytoplasm in many ameboid cells has been characterized as a viscoelastic material whose properties are dominated by actin filaments, intermediate filaments and microtubules, collectively termed the cytoskeleton (Janmey, 1991). Actin filaments are organized either as a meshwork in the leading edge, or as transient bundles of actin filaments that extend along the length of cells. These bundles may be attached to focal contacts, which anchor the bundles to the plasma membrane. Focal contacts facilitate attachment of the cell to the substratum, and allow cells to exert traction on the substrate. The elastic modulus of actin solutions is concentration dependent (MacKintosh, 1998), and they exhibit strain hardening (Xu *et al*., 2000), a property that may be important in movement of multicellular tissues. The cytoplasm in Dd has been characterized as an 'active viscoplastic' material (Feneberg and Westphal, 2001), because it exhibits viscoelastic behavior above a yield stress, but little deformation below this level. Several types of myosin are also important in Dd motility. Type I myosins, especially Myo A and Myo B, regulate the number and spatial localization of pseudopods (Gliksman *et al*., 2001). The cytoplasm of other cell types has similar properties: it is viscoelastic in leukocytes and neutrophils (Evans and Yeung, 1989; Heidemann *et al*., 1999; Yanai *et al*., 1999), but large regional variations in elasticity and viscosity coefficients are found within a cell (Yanai *et al*., 1999). Other cells may be more complex, e.g., endothelial cells have been modeled as hyperelastic materials and the nucleus and cytoplasm treated as distinct phases (Caille *et al*., 2002). It was found that the elastic moduli of the former is approximately ten times that of the latter.

1.1. ***Models of cell motility.*** Numerous models of cell motility have been proposed. Lauffenburger (1989) studied a one-dimensional model of the cell, regarded as three regions corresponding to the lamellipod, the cell body, and the uropod. The analysis focused on how the cell speed depends on receptor density and affinity. DiMilla *et al*. (1991) analyzed a one-dimensional model in which a cell consisted of discrete subunits, each with an elastic spring, dash-pot and contractile element

connected in parallel. Interaction with the substrate was modeled by additional Maxwell elements at the front and rear. The movement cycle was divided into three parts: the time needed for protrusion, the time of cytoskeleton contraction, and the time for cytoskeleton relaxation. These authors show that the observed bell-shaped distribution of the cell speed on the cell–substrate adhesiveness can be explained by an asymmetry in adhesiveness that results from preferable binding at the cell front due to increased affinity/avidity of integrin receptors. In this model the contractile stress does not vary within the cell and the effect of cell–substrate adhesions on contractile properties of the cell is not included. There are multiple examples of its influence on cell motility (Chrzanowska-Wodnicka and Burridge, 1996; Howe *et al*., 1998; Bershadsky and Geiger, 1999; Defilippi *et al*., 1999; Felsenfeld *et al*., 1999; Kaverina *et al*., 2002), and it is important to include this aspect in a model.

A 1D model for the steady gliding movement of fish keratocytes was developed in Mogilner *et al*. (2000), where it was shown that the dynamics of self-alignment and contraction of the actin–myosin network can explain forward translocation of the cell body. A model to describe the crawling movement of the sperm nematode was also developed recently. The model consists of a system of coupled differential equations that describe cell protrusion, contraction and adhesion, and under suitable biochemical regulation it produces steady motion of the cell (Mogilner and Verzi, 2002). A two-phase flow model of cytoplasm designed to understand cytoplasmic streaming and oscillations was studied in Alt and Dembo (1999).

A model for the movement of Dd cells, either as individuals or collectively as aggregates, was developed in Palsson and Othmer (2000). There a cell is modeled as a deformable ellipsoid of constant volume that contains a nonlinear spring in parallel with a Maxwell element along each axis of the ellipsoid. Restriction of the deformations to those that maintain an ellipsoidal shape enables large-scale computations to be done. Cell–cell and cell–substrate interactions, as well as reorientation of cells in response to a chemotactic signal was incorporated into the model. It was shown that the model can predict much of the behavior observed in two-dimensional Dd slugs (Bonner, 1998).

There are several other approaches to modeling cell deformations using a continuum description. The most widely-used is the 'cortical shell-fluid core' (CSFC) model (Yeung and Evans, 1989; Skalak *et al*., 1990; Schimd-Schönbein *et al*., 1995), in which the cortex is treated as a prestressed elastic medium and the core is treated as a fluid. This has been successful in explaining aspiration experiments (Yeung and Evans, 1989) and large, axisymmetric deformations of leukocytes (Dong and Skalak, 1992), but to date there is no 3D model based on the CSFC model of a cell that incorporates active forces and arbitrary shape changes.

More recently a method based on Voronoi diagrams for solving reaction–diffusion equations on irregularly-shaped, deforming domains has been developed and applied to a 2D model of nematode sperm (Bottino *et al*., 2002). The mechanical framework consists of a 2D mesh of nodes connected by edges that contain elastic elements in parallel with a contractile element. The interaction between the cell

and substrate was modeled by a viscous drag between cell body nodes and the substrate. Formal rules were applied to model actin polymerization at the leading edge and disassembly of the actin network at the rear of the cell, and the model was applied to both single cells and interacting cells. This approach was used in a new model developed recently to describe the crawling movement of the sperm nematode. This model consists of a system of coupled differential equations that describe cell protrusion, contraction and adhesion (Mogilner and Verzi, 2002). The above mentioned stages were biochemically regulated, and when solved together gave steady motion of the cell.

These models, with the exception of Mogilner and Verzi (2002), which is essentially a model of a single lamellipodial bundle, treat the cell body as a collection of a (usually) small number of springs and dashpots, and solve the resulting force balance equations at each node. While this approach provides qualitative insight into some features of the cell's motility, the cell body is more accurately described as a possibly multi-phase continuum, and therefore it is appropriate to model motility of cells by means of the continuum model. In the present paper we develop a continuum model of a cell as a viscoelastic material. Spatial variability in viscosity and elasticity coefficients along the cell body, together with a gradient in physical properties of the cell substratum attachments can be readily included in the model. This allows us to model different types of cells: for example, one choice of mechanical parameters exhibits features of a crawling fibroblast with elongation and release of the cell's tail (a 'pulsatile' motion), while another set of parameters can describe the steady gliding motion of a keratocyte. The nucleus can also be treated as another viscoelastic or purely viscous substance embedded in the cell body.

The objectives here are twofold.

(1) To develop a one-dimensional cell model that includes essential components of motility such as the actin cytoskeleton, myosin II-based contraction of the actin cytoskeleton, and cell–ECM adhesion. The model cell that we consider consists of a viscoelastic cytoskeleton that can produce an active protrusive force due to actin polymerization and a contractile stress due to myosin II motors. The cell interacts with the substrate by means of adhesion mediated by integrin receptors.

(2) To use this model to interpret experimental results on the motion of certain cell types. A one-dimensional model with active force production is not suitable for the description of all cells: for example, keratocyte movement is inherently two-dimensional because on average this cell generates active forces orthogonal to the direction of motion. On the other hand, a fibroblast is known to generate myosin II-powered contraction aligned with the direction of locomotion (Munevar *et al*., 2001a,b). Thus, we shall apply the model to a fibroblast cell and in particular, we shall explain the traction patterns observed experimentally (Dembo and Wang, 1999; Munevar *et al*., 2001a,b). We also study the dependence of the cell velocity v on the substrate ligand concentration n_s, and compare it to the experimentally-observed 'bell-shaped curve' (Palecek *et al*., 1997), and we make predictions on

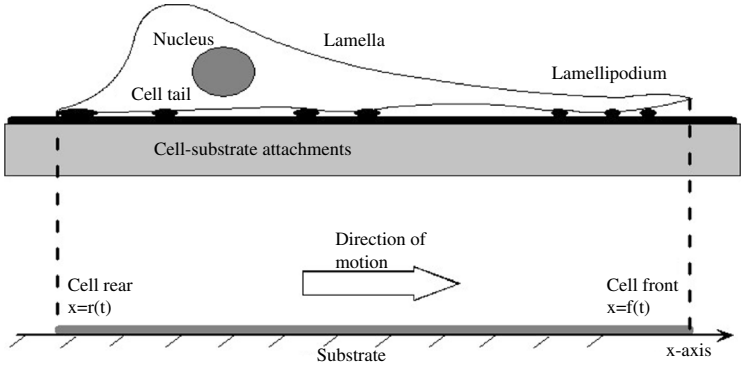

Figure 1. Schematic of the one-dimensional model cell. Actin polymerization occurs in the cell lamellipodium. $f(t)$ denotes the position of the leading edge and $r(t)$ the position of the trailing edge of the cell.

how cell properties may change the bell-shaped curve of $v(n_s)$; to discuss the model consequent results for 'bistability'—stimulus induced switching of stationary cell into the locomoting one (Verkhovsky *et al.*, 1999).

The paper is organized as follows. In the following section we develop the continuum model of cell motion. In Section 3 we apply it to fibroblasts and compare our results with available experimental data on the distribution of traction forces and cell velocity curves. In Section 4 we discuss future applications of the model.

2. Cell Model

2.1. ***The equations of motion.*** We consider a one-dimensional viscoelastic cell with initial length L in contact with a viscous substrate, as shown in Fig. 1. Define a coordinate system that is attached to the stationary substrate, and denote the initial position of the cell by a set of points with coordinates $0 \leq x \leq L$. Further, denote the position of the cell front (rear) by $f(t)$ $(r(t))$, so that at any time t a cell is represented by a set of points that belong to the interval $r(t) \leq x'(x,t) \leq f(t)$ (Fig. 1). The displacement u of the cell from the configuration x is defined as [see, e.g., Landau and Lifshits (1965) for details]

$$u(x,t) = x'(x,t) - x. \tag{1}$$

In formulating the equation of motion we neglect inertial effects and body forces. The former may be important during the brief, rapid acceleration and deceleration that occur during lamellipod extension (Felder and Elson, 1990), but are otherwise negligible. Then the forces on a cell are the internal active and passive stress, and the frictional force due to the repetitive formation and breaking of attachments to the substrate. Let σ denote the Cauchy stress, i.e., the stress in the present configuration: then the evolution of the deformation is governed by the equation

$$\frac{\partial \sigma}{\partial x} = \beta(x)\frac{\partial u}{\partial t} \tag{2}$$

where the right-hand side of the equation describes the viscous interaction of the cell with the substrate and $\beta(x)$ is the friction or drag coefficient, with units of M/L^3T.

We describe the cytosol, including the actin filaments, microtubules and intermediate filaments, as a linear viscoelastic material that gives rise to a passive stress, an active protrusive stress due to actin polymerization concentrated at the leading edge, and an active stress generated by the interaction of myosin II motors with the cytoskeleton. Then the total stress σ is the sum of a passive stress (elastic stress plus viscous stress) and the active stress $\tau(x)$, and can be written*

$$\sigma = E(x)\varepsilon + \mu(x)\frac{\partial \varepsilon}{\partial t} + \tau(x), \tag{3}$$

where $\varepsilon = \partial u/\partial x$ is the small-deformation strain, and $E(x)$ and $\mu(x)$ are the elastic modulus and the viscosity coefficient, respectively. If the viscoelastic material is considered to be fluid-like (corresponding to the Maxwell fluid model rather than the Kelvin–Voight model that is equivalent to our formulation), another constitutive equation must be used.

To complete the formulation of the problem, we specify boundary conditions for (2) which represent force balances at the leading and trailing edges. The former equates the internal stresses to the force due to actin polymerization, which is concentrated at the leading edge, while the latter stipulates that the internal stresses vanish at the trailing edge. Thus we specify that

$$\left[E(x)\varepsilon + \mu(x)\frac{\partial \varepsilon}{\partial t} + \tau(x)\right]\Big|_{f(t)} = F_f, \tag{4}$$

$$\left[E(x)\varepsilon + \mu(x)\frac{\partial \varepsilon}{\partial t} + \tau(x)\right]\Big|_{r(t)} = 0, \tag{5}$$

where F_f is the force due to the actin polymerization. This force is estimated in the Appendix B.

2.2. *Constitutive assumptions*

2.2.1. *Actin dynamics and viscoelastic properties.* The elastic modulus and viscosity of the cytosol depend on three factors: the actin network, the microtubules, and the intermediate filaments. The actin network is a main component of cytoskeleton, with microtubules and intermediate filaments providing the additive constants to the overall cytoskeleton elasticity. While the overall processes

*In this formulation the additivity of the component stresses corresponds to a discrete model in which the elastic elements (springs) and viscous elements (dashpots) are connected in parallel.

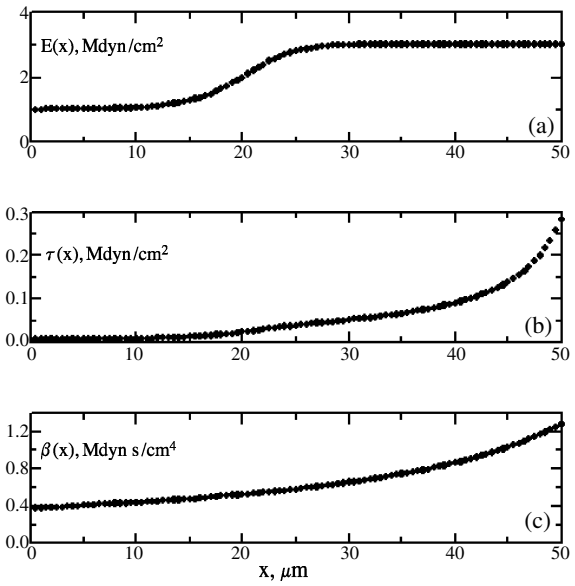

Figure 2. (a) The assumed cell elasticity $E(x)$, (b) the computed active stress $\tau(x)$, and (c) the cell–substrate drag coefficient $\beta(x)$, as functions of position x along the cell. The computed form of the contractile stress $\tau(x)$ is similar to that observed in Munevar *et al.* (2001a), where most of the cell motors are activated at the front of the cell. The choice of cell elasticity $E(x)$ is motivated by the presence of the nucleus in the middle of the cell and a denser actin-based network in the lamellipodium. The calculated cell–substrate interaction $\beta(x)$ exhibits the axial asymmetry seen experimentally. The distributions are shown for $t = 0$ min. $\kappa_s = 0.05$, and other parameters are given in Tables 1 and 2.

involved in forming the network by actin polymerization are known, many details of the control of these processes are not. Many auxiliary proteins are involved, in capping of barbed actin filamental ends as well as in WASP/Arp2/3-mediated branching of actin filaments. We do not incorporate a detailed description of the dynamics of actin network formation here, but the reader can find a detailed model for actin polymerization in Mogilner and Edelstein-Keshet (2002). We assume that the spatial distribution of actin network density is time-independent, and we represent the elasticity as

$$E(x) = E_0 a(x), \tag{6}$$

where $a(x)$ is the actin network density and E_0 is a proportionality constant. We use the specific form of $E(x)$ that is shown in Fig. 2(a). This choice is motivated by the observation that the central region of the cell (the nuclear region) seems to have more rigid properties than the cell rear, due to the denser cytoskeleton. The leading edge also may be softer then the surroundings, in particular in a thin lamellipodial strip of 1–5 μm width where the actin is polymerized, but we do not incorporate this here. We also do not consider the spatial variation of viscosity μ.

2.2.2. *Integrin dynamics.* The force on the right-hand side of (2) describes the cell–substrate interaction, which arises from adhesion via, e.g., integrins. A molecular-level analysis of the forces involved and the lifetime of individual bonds was done by Bell (1978), and since then there have been many models of the adhesion process. Usually a cell has a small number of adhesion sites, of the order of a hundred to a thousand, each of which can be described as a viscoelastic element that connects the cell with the substrate (Ragsdale *et al*., 1997; Heidemann *et al*., 1999), and which can be modeled as a viscoelastic slip element. In a discrete mechanical model each element will consist of a spring with spring constant E_0 and zero equilibrium length (the elastic element) and a dashpot with viscosity β (the viscous element) connected in parallel. However, in the continuum model developed here we describe the effect of the cell–substrate adhesion sites through an effective drag coefficient β as a linear function of the attached integrin density $n_b(x)$, i.e.,

$$\beta(x) = \beta_0 n_b(x), \tag{7}$$

where β_0 is a time-averaged drag created by one integrin receptor bound to the substrate.

Let n_f be the density of free integrins in the membrane and let n_b be the density of integrins bound to the substrate ligands. Suppose that bonds form with a rate k_f and dissociate with a rate $k_{r0} f_1(x)$ that varies with position along the cell. The ligand concentration in the substrate n_s is taken to be uniform, and large enough to ignore depletion due to binding of n_s. Suppose that the total number N_{total} of integrin receptors in the cell is constant and that diffusion of receptors is negligible. Then at steady state the density of free integrins n_f is a constant that is determined from the conservation condition, and

$$n_b(x) = \frac{k_f n_s}{k_{r0} f_1(x)} n_f = \frac{\kappa_s}{f_1(x)} n_f, \tag{8}$$

where $\kappa_s = k_f n_s / k_{r0}$ is a dimensionless coefficient for cell–substrate interaction. Then the drag coefficient is

$$\beta(x) = \beta_0 n_b(x) = \beta_0 \frac{\kappa_s}{f_1(x)} n_f, \tag{9}$$

and we further assume that

$$f_1(x) = \psi_1 + (1 - \psi_1)\frac{x - r}{f - r}, \tag{10}$$

where $\psi_1 \geq 1$ describes the linear increase of dissociation rate towards the rear. Consequently, $f_1 = 1$ at the front of the cell and $f_1 = \psi$ at the rear of the cell. The x-dependence of the drag coefficient used later is shown in Fig. 2(c).

2.2.3. *Contractile stress due to myosin II.* Next we consider the contractile stress generation in more detail. The contractile component describes the tension in the actin–myosin network that is regulated by different proteins. For example, an increase of the protein *Rho* is followed by an increase in cell tension (Hollenbeck, 2001). Another protein, *Rac*, regulates production of pseudopodia, in part via regulation of actin polymerization: an increase in *Rac* production leads to an increase in pseudopodia formation. Interaction of *Rac* and *Rho* also affects microtubule growth, and thereby tension in the cell cortex (Hollenbeck, 2001; Kaverina *et al*., 2002; Wood and Martin, 2002).

Let m_f denote the concentration of free myosin II, m_b the concentration of inactive bound myosin II in the cytoskeleton, and m_b^+ the concentration of active bound myosin II. We assume that $\tau(x)$ is proportional to the concentration of the bound active myosin II $m_b^+(x)$. The latter increases in response to extracellular signals, release of bound myosin into free myosin, and activation of myosin II. The total amount of myosin II M_{total} in a cell is conserved.

It has been shown that propulsive forces for cell migration are concentrated at the leading edge in the cell lamellipodium (Munevar *et al*., 2001a). The authors conclude that the anterior region of the cell and the remainder of the cell are mechanically distinct domains. These experiments also showed that forces near the tail of a locomoting fibroblast are of a passive type; in other words the cell tail serves only as a site of passive anchorage. They proposed that the leading lamellipodium consists of one or more 'towing zones', connected to the cell body via an elastic transition zone, and generation/transmission of contractile forces in the towing zones provides the forces responsible for towing the cell body and passive trailing end (Munevar *et al*., 2001b).

In accord with this description, we assume that the rate of activation of bound myosin II, k_{Reg}^+, is position dependent and is given by the linear function

$$k_{\text{Reg}}^+(x) = k_{\text{Reg}}^+ f_2(x) = k_{\text{Reg}}^+ \Big/ \left[\psi_2 + (1-\psi_2)\frac{x-r}{f-r}\right], \tag{11}$$

where $\psi_2 \geq 1$. Therefore $k_{\text{Reg}}^+(f) = k_{\text{Reg}}^+$ at the front and $k_{\text{Reg}}^+(r) = k_{\text{Reg}}^+/\psi_2$ at the rear of the cell. The kinetics of activation are assumed to be fast and therefore

$$m_b(x) = \frac{k_m^+}{k_m^-} a(x) m_f, \tag{12}$$

$$m_b^+(x) = \frac{k_{\text{Reg}}^+ f_2(x)}{k_{\text{Reg}}^-} [\text{Reg}] m_b(x). \tag{13}$$

Here k_m^+ is rate of myosin binding, k_m^- is the rate of decay of bound myosin, k_{Reg}^+ is the rate of activation of myosin II due to a regulatory protein of concentration [Reg], and k_{Reg}^- is rate of deactivation of myosin II.

We assume that the formation of adhesion sites influences active stress generation through this regulatory protein, and its 'production' is related to the integrin concentration via

$$[\mathrm{Reg}] = [\mathrm{Reg}]_0 \frac{n_b^\alpha}{n_{b0}^\alpha + n_b^\alpha} = [\mathrm{Reg}]_0 f(n_b), \tag{14}$$

where $[\mathrm{Reg}]_0$ is maximum level of regulatory protein, n_{b0} is typical concentration of bound integrins and α is a degree of coupling between regulatory protein and integrins. Finally, we assume that the active stress tensor τ depends linearly on m_b^+

$$\tau(x) = -\tau_0 m_b^+(x), \tag{15}$$

where τ_0 is magnitude of the stress generated by one acto-myosin bundle. The x-dependence of the active stress used later is shown in Fig. 2(b). The asymmetry in active force generation postulated is supported by experimental results (Munevar *et al*., 2001a), where release of posterior adhesions resulted in no significant decrease of traction forces, whereas release of the frontal lamellipodial region resulted in a dramatic decrease of traction forces. This effect may be explained as follows. Since contractile stress is concentrated in the cell front and there is no active stress at the anterior end, the release of the rear has no effect on average active stress, but the release of the anterior part, where most of the active stress is concentrated, is followed by a decrease in active stress, and as a result, the cell average traction stress decreases dramatically. This experiment shows that not only is the cell–substrate interaction asymmetry important, but also an asymmetry of the cell contractile stress generation is needed.

3. Application of the Continuum Model to a Fibroblast Cell

In this section we apply the general model to fibroblasts, which are a widely-studied type of motile epidermal cell. Fibroblasts are slowly-moving cells that move with an average velocity of about 0.5 μm min^{-1} (Lo *et al*., 2000; Munevar *et al*., 2001a,b; Wang *et al*., 2001). One objective is to understand from a a simple model how fibroblasts interact with the substrate and how specific traction patterns are formed (Lo *et al*., 2000).

We compare results of our model with experimental data of Dembo and Wang (1999) and Munevar *et al*. (2001a,b), where the mechanical interaction of the cell with a substrate was studied using traction force microscopy. This allows visualization of the deformations in the substrate that result from mechanical forces exerted by the fibroblasts on it [see Fig. 1 in Munevar *et al*. (2001b)]. The experiments were done on fibroblast cells deposited on a polyacrylamide substrate embedded with fluorescent beads. First cells were allowed to attach and spread on the

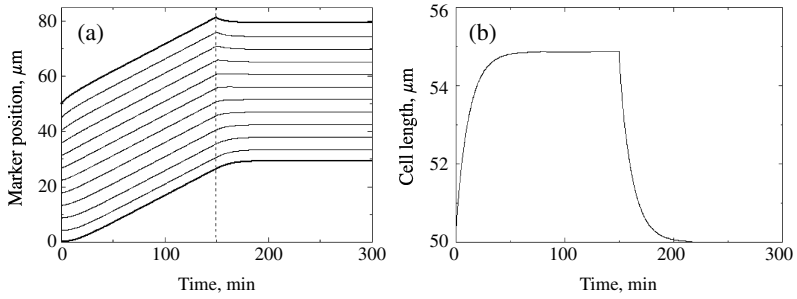

Figure 3. (a) The calculated positions of the leading and trailing edges of the cell, together with the positions of internal marker particles as functions of time. A stable cell length ∼55 μm and a cell velocity $v = 0.19$ μm min^{-1} are established after an initial period. (b) The cell length as a function of time. At $t = 150$ min the contractile stress $\tau(x)$ is set to zero [dashed vertical line in (a)] to simulate cell relaxation experiments, and by $t =\sim 300$ min the original cell length 50 μm is reached. Here $\kappa_s = 0.05$ and other parameters are as given in Tables 1 and 2.

substrate and then were micro-injected with Gc-globulin, an actin cytoskeleton inhibitor that relaxes the cytoskeleton and prevents force generation by cells. Deformation of the substrate was determined by comparing the distribution of microspheres before and after cell force relaxation. The traction field can be computed knowing the displacements by solving an inverse problem.

3.1. ***Fixed substrate density.*** Cell motion entails variations in the length of the cell, its velocity, areas of cell cytoskeletal stretch or compression, and a field of traction forces generated by the cell. Variations in these output characteristics of the model can be achieved by (i) exploring different initial lengths of the cell, (ii) varying the elastic and contractile properties of the cell (the magnitude and distribution throughout the cell), (iii) variation of substrate properties, and (iv) changing the boundary conditions at the front and rear of the cell. The computational details for solution of equations (2)–(5) and equations (6), (9) and (15) are given in Appendix A.

Fig. 3(a) shows the distance traveled by the model cell as a function of time, beginning with a length of $L = 50$ μm. In this plot the top line represents the position of the front and the bottom line the rear of the cell. Thin lines between them represent the positions of marker particles in the cell. In Fig. 3(b) we see that after $t \sim 70$ min the length of the cell reaches a steady-state value. In this example the steady-state cell speed is 0.19 μm min^{-1} and the corresponding cell length is approximately 55 μm, which compares well with experimental observations (Lo *et al.*, 2000; Munevar *et al.*, 2001a,b; Wang *et al.*, 2001). To model the experimentally-induced relaxation of the cytoskeleton, we set the active stress $\tau(x) = 0$ at $t = 150$ min (see Fig. 3). With no active force generation (or more generally, no asymmetry in active force generation), motion ceases and the cell relaxes to its initial length of 50 μm [see Fig. 3(b)].

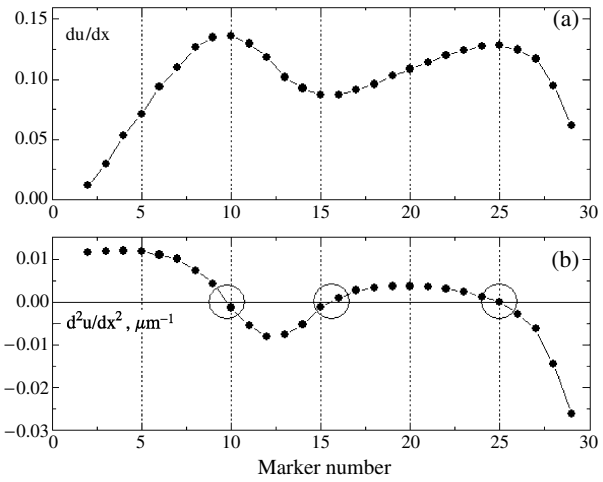

Figure 4. (a) The computed cell strain $\varepsilon = \frac{\partial u}{\partial x}$ as a function of the marker position in the cell body. The first (last) marker coincides with the posterior (anterior) edge of the cell. (b) The computed value of $\frac{\partial^2 u}{\partial x^2}$ as a function of the marker position in the cell body. Both graphs are calculated at $t = 150$ min and $\kappa_s = 0.05$, and other parameters are as given in Tables 1 and 2.

The calculated deformation gradient (strain) of the cell $\varepsilon = \partial u/\partial x$ at $t = 150$ min (just prior to turning off the active force) is shown in Fig. 4(a). The maximum deformation shown there has a magnitude $\sim$0.15, and if a nonlinear strain tensor is used the next term is $\sim(0.15)^2/2 \sim 0.01$, which is small compared to deformation itself. This provides *a posteriori* justification for the use of the linear approximation for the strain in the model.

In the experimentally-inferred traction field of the fibroblast (calculated from the displacement of marker beads embedded in the substrate), the lamellipodial region can be divided into multiple domains separated by regions of high shear (Munevar *et al*., 2001b) in which the traction force changes direction. The computed traction forces were low in the middle of the cell, beneath the nucleus, while large magnitudes were observed in lamellipodium (in a band of $\sim$15 μm in width), where forces were oriented opposite to the direction of the cell locomotion, and at the tip of the cell's tail where they were aligned in the direction of locomotion.

In the model the displacement of the marker particles in the cell is large at the front of the cell, changes sign three times (shown by circles) and becomes large again at the cell rear (Fig. 4). These changes coincide with the regions of rapid change in either the elastic coefficient or the drag coefficient. This is similar to the experimentally-observed changes in the substrate displacement but cannot be compared directly because under steady-state conditions it follows from the equation of motion that the force exerted by the cell on the substrate is a linear function of position along the cell. The pulsatile motion more characteristic of fibroblast motion is discussed later. The experimentally-observed region of small traction stresses is

located in the vicinity of the nucleus (Munevar *et al*., 2001b). Note that to obtain more pronounced regions of small traction forces with opposite directions of traction vectors in the middle of the cell (in the vicinity of the nucleus), one could model the nucleus as an incompressible or a very stiff material. It is known that the elastic modulus of the nucleus is nearly ten times higher that the cytoskeleton (Janmey, 1998). On the other hand, recent experiments show (Nagayama *et al*., 2001) that nucleus stiffness decreases dramatically in locomoting cells, whereas in stationary cells it remains larger than the stiffness of the surrounding cytoskeleton. It is possible to incorporate this in our model.

It can be concluded from our calculations, that distinct regions in the field of traction stresses that were experimentally observed (Munevar *et al*., 2001b) depend on local interplay between elastic and contractile properties of the cell cytoskeleton at a given location inside the cell as well as cell–substrate interactions.

It was also found that although forces generated by H-ras transformed 3T3 cells become radially symmetric, these cells retain the ability to locomote with average velocities greater that those of normal fibroblast cells (Munevar *et al*., 2001b). As it was suggested in that work, this can be explained by the disruption of focal adhesion kinase (FAK) in the transformed cell. Increased motility of the cells with disrupted adhesions (weaker cell–substrate adhesion) can be explained in the frames of our model. Our simulation results suggest that significant disruption of cell–substrate adhesions is necessary for the model cell to retain the ability to move. The disruption of the adhesions, in turn, leads to a significant reduction of the active stress magnitude, followed by reduction of traction forces and more compact cell shape. This will be considered further in the following section.

Because we have modeled the cell substrate interactions as a viscous interaction, there is no variation in the cell length after the cell reaches a steady motion regime, in contrast with the experimentally-observed motion of fibroblasts, which move in a pulsatile manner. This can be easily remedied by including discrete adhesion sites throughout the cell, with a threshold force for release at an adhesion site. To demonstrate this effect we added to the original model one elastic element with a threshold for detachment at the rear. In Fig. 5 we show the front and rear positions of the cell computed using the continuum model [arrows (1)], and the front and rear positions of the cell with an additional elastic element with a threshold for breakage [arrows (2)]. The addition of this elastic element gives rise to cycles of sticking and slipping at the rear, according to whether the local force is below or above threshold. The average cell speed remains constant, but the rear goes through repeated cycles of zero/nonzero speed values (see Fig. 5).

3.2. ***The effect of varying parameters in the model.*** Palecek *et al*. (1997) measured the dependence of cell speed on a variety of properties that characterize the cell–substrate interaction. Different expression levels of integrin receptors were studied, as well as integrin–ligand affinities, and it was shown that cell speed is a

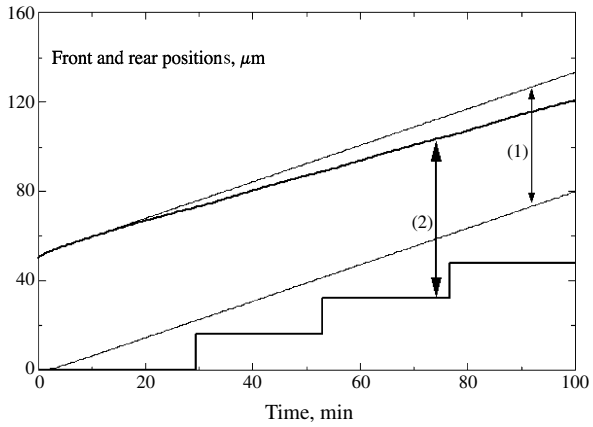

Figure 5. The calculated positions of the posterior and anterior of two model cells as functions of time: (1) in the continuum model with viscous cell–substrate interaction at steady state; (2) in the continuum model with viscous cell–substrate interaction and an elastic element with a threshold at the posterior end. The threshold for release in the attachment is adjusted to obtain the typical duration of a fibroblast cycle, which is 30 min. The presence of this additional element leads to the appearance of pulsatile cell elongation and retraction, as observed in fibroblast cells. Here $\kappa_s = 0.05$, and other parameters are as given in Tables 1 and 2.

bell-shaped function of fibronectin coating concentration. It was also found that maximum attainable cell speed is not a function of integrin expression or ligand affinities. These experiments suggested that integrin coupling with intracellular motors remains unaltered. These results are in qualitative agreement with the model due to DiMilla *et al.* (1991) discussed earlier.

The dependence of the cell velocity v as a function of cell–substrate interaction parameter κ_s predicted by the present model is shown in Fig. 6. This function has a bell-shaped form similar to those observed experimentally (Palecek *et al.*, 1997). On substrates with small κ_s the cell cannot effectively transmit force to the substrate, and the speed tends to zero. In the limit of large κ_s the contractile force cannot overcome the strong cell–substrate interaction and the cell remains stationary. Since the speed is nonnegative there must be at least one intermediate value of κ_s at which the speed is a local maximum. Our computations show that there is only one such point, and there the contractile force is comparable to the cell–substrate interaction, which results in optimal cell motion. Figure 6 also shows how cell length changes with value of κ_s. We note that there is no significant extension of the cell at small κ_s, it extends rapidly over a small range of κ_s, and finally, at large values of κ_s, stretching changes little with further increases in κ_s because the cell cannot overcome the strong adhesion forces. This behavior is also seen in experiments (Palecek *et al.*, 1997).

Since $\kappa_s \equiv k_f n_s / k_{r0}$, the effects of changing either of the on rate or the off rate, or of varying the density of adhesion sites on the substrate can be inferred

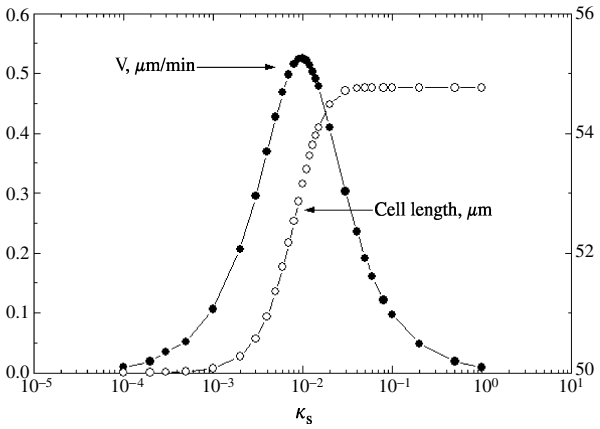

Figure 6. (•) The calculated cell speed v as function of the strength of cell–substrate interaction as measured by κ_s. The cell moves more efficiently at intermediate values of cell–substrate interaction. This bell-shaped distribution is similar to the one seen experimentally (Palecek *et al.*, 1997). (○) The calculated cell length as a function of cell–substrate interaction κ_s. The model cell has compact shape and small speed at small cell–substrate interaction. At average κ_s the cell stretches and moves with maximum speed. Finally, at large κ_s the cell cannot stretch any more and movement ceases. Parameters are given in Tables 1 and 2.

from Fig. 6. For example, increasing the off rate from low levels at fixed values of the other parameters corresponds to decreasing κ_s in Fig. 6.

Next we investigated the effect of the exponent α that is used in coupling function [Reg] [equation (14)]. As can be seen, the value of α shows how fast the regulatory protein concentration rises with the increase in bound integrin concentration. We found that as α increases, the maximum cell speed $v_{\max}$ attainable increases as well (Fig. 7). The distribution $v(\kappa_s)$ also becomes more narrow with increase of α.

Finally we consider the effect of viscoelastic properties on the cell motion. According to experiments, the viscosity of a fibroblast is small (see Table 1). In our model variation of the viscosity does not change results significantly at the moment of initiation of the motion, but if the model cell is very viscous it may influence cell behavior, for example, how fast the cell reaches equilibrium. However, changes in the elastic modulus have a more significant effect (cf. Fig. 8). These curves correspond to two different actin concentrations $A_{\text{total}} = 200$ and 400 μM and model two cells with different density of cytoskeleton. We find that a stiffer cell (with larger A_{total}) shows a larger speed at all values of κ_s (upper curve in Fig. 8). We are not aware of experiments in which the stiffness of the cytoskeleton has been varied, but some measurements of cell stiffness as a function of a position inside the cell can be found in Nagayama *et al.* (2001).

In our model, the activation of myosin II is connected with the density of the actin cytoskeleton, in that dense cytoskeleton promotes activation of myosin II. However, if the contractile stress generation is independent of cytoskeletal density

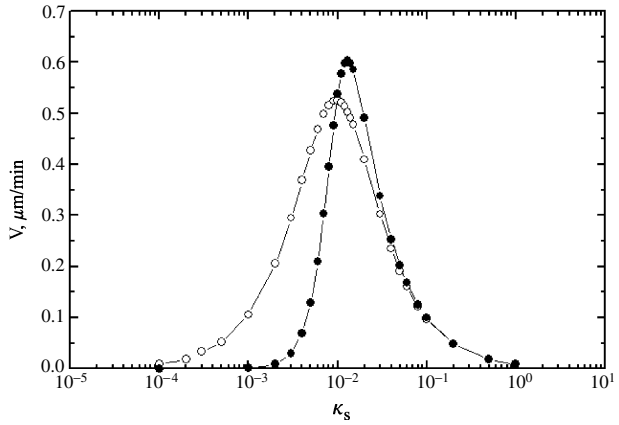

Figure 7. The calculated cell speed v as a function of κ_s for two different Hill coefficients α [see equation (14)] with $\alpha = 2$ (○) and 4 (●), other parameters as in Tables 1 and 2. An increase in α from 2 to 4 results in: (1) a shift of the speed distribution in the region of larger κ_s, (2) an increase in the maximum cell speed, and (3) a narrower speed distribution. Other parameters are given in Fig. 6.

Table 1. Cell parameters.

Parameter	Definition	Value	References
L	Cell length	50–70 μm	(Dembo and Wang, 1999; Lo *et al*., 2000; Munevar *et al*., 2001b)
h	Lamellipodium height	1 μm	This work
V	Cell volume	1000 μm^3	This work
μ	Cell viscosity	2.0×10^3 dyn s cm^{-2}	(Bausch *et al*., 1999)
E	Cell elasticity	$0.1–2.5 \times 10^7$ dyn cm^{-2}	(Wakatsuki *et al*., 2000)
f_0	Cell force	500–1000 nN	(Wakatsuki *et al*., 2000)
S_{cross}	Cell cross area	30–50 μm^2	(Dembo and Wang, 1999; Lo *et al*., 2000; Munevar *et al*., 2001b)
A_{total}	Total actin in polymerized form	200 μM	(Mogilner and Edelstein-Keshet, 2002)
M_{total}	Total myosin II	20.0 μM	This work
N_{total}	Total integrin	10^5 receptors/cell	(DiMilla *et al*., 1991)
k_{r0}	Dissociation constant	0.67 s^{-1}	(DiMilla *et al*., 1991)

or cell–substrate interaction, the cell velocity depends only on the ratio of contractile cell stress to cell–substrate interaction $\beta(x)$, as shown in Appendix C.

The maximum speed of the cell increases when the contractile force increases, as expected. This result is shown in Fig. 9, where the cell speed as a function of cell–substrate interaction parameter κ_s is shown for two different levels of contractile stress: $\tau_{max} = 1.0$ and 2.0 Mdyn cm^{-2}. Not only does the maximal attainable

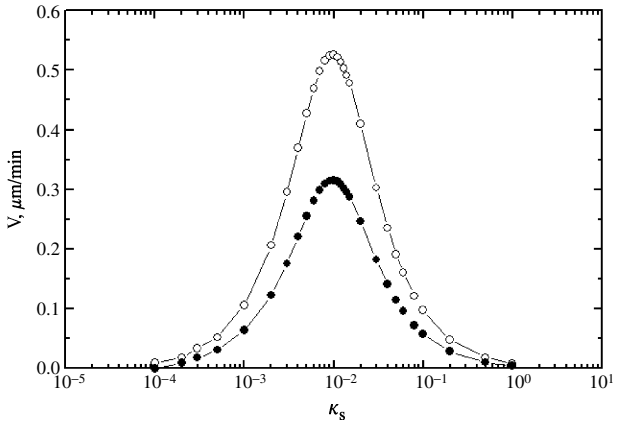

Figure 8. Cell speed as a function of κ_s for two model cells with two total actin densities $A_{\text{total}} = 400$ μM (○) and $A_{\text{total}} = 200$ μM (●); other parameters are given in Tables 1 and 2.

speed grow with the increase of τ, but the width of the distribution increases as well. This means that a cell with greater cell contractility may crawl over a wider range of substrates.

4. Conclusion

We have developed a continuum model describing the motion of a single cell that consists of a mechanical cell model regulated by the essential cell motility proteins. In this model the mechanical properties of the cell, such as the cell elasticity, contractile ability and cell–substrate interaction are governed by the distributions of the corresponding proteins. Thus, cell elasticity is primarily controlled by the actin cytoskeleton, the cell contractile force generation is connected to myosin II motors, and the cell–substrate interaction is mediated by integrin dynamics.

The continuum model is applied to describe the motion of a fibroblast. The model introduces a feedback mechanism between cell–substrate interaction and contractile force generation. It is assumed that strong cell–substrate adhesion at the cell frontal part promotes activation of myosin II. This assumption is supported by experimental observations of traction stresses in fibroblasts (Munevar *et al.*, 2001a), as well as experimental observation of MLCK activation in the lamella (Chew *et al.*, 2002). It is most likely that in live cells the 'asymmetry' much needed for cell motility arises from both discussed factors: cell–substrate adhesion asymmetry and cell contractile ability, which in turn is influenced by cell–substrate interaction.

The solution of the model equations allows us to obtain the cell deformation, speed and strain. According to our calculations, the model cell has several areas of cell stretch and compression. We also simulated the experiment of Munevar *et al.* (2001b) to obtain traction stress. In agreement with the experimental data,

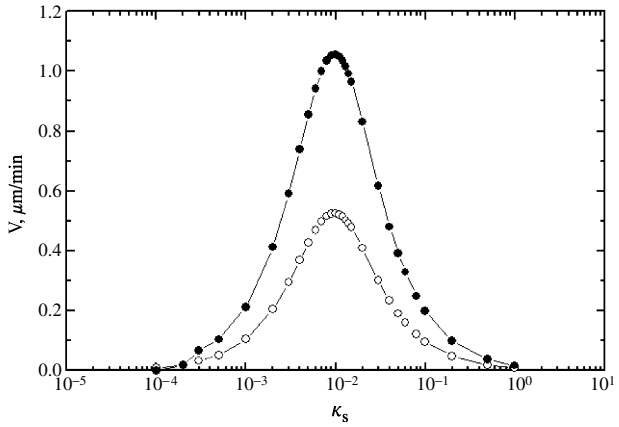

Figure 9. Two velocity vs. κ_s curves for two different maximum levels of contractile stress: $\tau_{\max} = 1.0$ Mdyn cm^{-2} (○) and $\tau_{\max} = 2.0$ Mdyn cm^{-2} (●), other parameters are given in Tables 1 and 2.

the calculated traction stress is large and negative at the cell front and large and positive at the cell rear.

In addition, we were able to obtain the bell-shaped distributions of the cell speed as a function of cell–substrate interaction similar to those experimentally observed (Palecek *et al*., 1997). Corresponding cell stretch calculated as a function of the cell–substrate interaction is also in agreement with experimental situation. The model cell does not stretch much at small values of cell–substrate interaction, it stretches more at intermediate values and reaches maximum length at large values of cell–substrate interaction.

Our model can be easily applied to simulate locomotion of different cells and accounts for a variety of cell motion types. In order to describe the desired cell, it is necessary to incorporate the appropriately defined elastic and viscous properties as well as active contractile stress specific to a given cell type. The discussed model may be applied to study motility of different cell types (fibroblasts, neutrophils, epithelial cells and others); to study the movement of the ameboid cells and cell aggregates (such as slug movement of *Dd*); to study mechano-transduction (such as stretch-activated calcium channels in different cell types, integrin dynamics and mechano-sensing at the adhesion sites), and so on. The work on a two-dimensional model is currently underway.

ACKNOWLEDGEMENTS

This work was supported by grants NSF-DMS0096312 and NIH-GM29123. We would like to thank Alex Mogilner and Juliet Lee for discussions on the subject and Magdalena Stolarska for a careful reading of the manuscript.

APPENDIX A: COMPUTATIONAL DETAILS

We compute protein concentrations by setting $f = f(0) = L$ and $r = r(0) = 0$ in corresponding equations, assuming that the cell deformation has little influence on the protein dynamics.

According to our model cell elasticity $E(x)$ is proportional to bound actin density in the cytoskeleton, cell active stress $\tau(x)$ is proportional to bound active myosin II density and cell drag coefficient $\beta(x)$ is proportional to bound integrin density. A typical result is presented in Fig. 2 where the dependencies of the cell elasticity, cell active stress and cell drag coefficient are shown as functions of position inside the cell. Note, that the calculated bound active myosin II density is qualitatively-similar to the observed activity of *MLCK* in Chew *et al*. (2002). Using these material properties, equations (2)–(5) are solved for the displacement $u(x, t)$. The positions of the leading edge $f(t)$ and the rear of the cell $r(t)$ at the next moment of time are determined from the following conditions on the speed of the cell at the front and rear:

$$f(t) = L + u, \tag{A.1}$$

$$r(t) = u. \tag{A.2}$$

Equations (2)–(5) were numerically integrated using an explicit scheme in time and generalized Gaussian method to solve for the displacements $u(x, t)$ on the grid with initial spacing $\delta = 0.5\ \mu$m (Samarsky, 1983; Sod, 1985). We took the time step to be small enough (typically $\Delta t = 10^{-3}$ s) to maintain stability. Initial displacements $u(x, t = 0)$ were assumed to be zero, cell rear boundary is at the origin of coordinate system $r(0) = 0$ and cell front is at $f(0) = L$.

We discretize equation (3) in the following way, where indexes i and j signify the discretization in space and time correspondingly:

$$\frac{\partial}{\partial x}\left(E(x)\frac{\partial u}{\partial x}\right) = \frac{E^j_{i+1/2}}{\Delta x}\left(\frac{\partial u}{\partial x}\right)_{i+1/2} - \frac{E^j_{i-1/2}}{\Delta x}\left(\frac{\partial u}{\partial x}\right)_{i-1/2} \tag{A.3}$$

$$= \frac{E^j_{i+1/2}}{\Delta x}\frac{(u^j_{i+1} - u^j_i)}{\Delta x} - \frac{E^j_{i-1/2}}{\Delta x}\frac{(u^j_i - u^j_{i-1})}{\Delta x} \tag{A.4}$$

$$= \frac{E^j_{i+1/2}}{(\Delta x)^2}u^j_{i+1} - \frac{E^j_{i+1/2} + E^j_{i-1/2}}{(\Delta x)^2}u^j_i + \frac{E^j_{i-1/2}}{(\Delta x)^2}u^j_{i-1}, \tag{A.5}$$

where

$$E^j_{i+1/2} = \frac{E^j_{i+1} + E^j_i}{2}, \qquad E^j_{i-1/2} = \frac{E^j_{i-1} + E^j_i}{2}, \tag{A.6}$$

Table 2. Cell model parameters.

Parameter	Definition	Value
κ_s	Cell–substrate interaction	10^{-4}–10^{2}
ψ_1	Front–rear dissociation asymmetry	3.33
κ_m^+/κ_m^-	Association/dissociation rate ratio	0.3
$\kappa_{\mathrm{Reg}}^+[\mathrm{Reg}]_0/\kappa_{\mathrm{Reg}}^-$	Association/dissociation rate ratio	0.1
α		2.0
ψ_2	Front–rear myosin II activation asymmetry	10.0
E_0	Cell elastic constant	0.42×10^{-8} dyn μm^{-1}
τ_0	Active stress constant	4.2×10^{-8} dyn μm^{-1}
μ	Cell viscosity constant	10^{-11} dyn $\cdot$ s μm^{-1}
β_0	Drag constant	5×10^{-10} dyn s μm^{-3}

$$\mu \frac{\partial}{\partial t}\frac{\partial^2 u}{\partial x^2} = \mu \left[\frac{u_{i+1}^j - 2u_i^j + u_{i-1}^j}{\Delta t(\Delta x)^2} - \frac{u_{i+1}^{j-1} - 2u_i^{j-1} + u_{i-1}^{j-1}}{\Delta t(\Delta x)^2} \right], \tag{A.7}$$

$$\frac{\partial \tau}{\partial x} = \frac{\tau(x_{i+1}^j) - \tau(x_{i-1}^j)}{2\Delta x}, \tag{A.8}$$

$$\beta(x)\frac{\partial u}{\partial t} = \beta(x)\frac{u_i^j - u_i^{j-1}}{\Delta t}. \tag{A.9}$$

Appendix B: Model Parameters

Recently-developed experimental techniques such as magnetic traps, magnetic tweezers (Bausch *et al.*, 1999), micromachinery devices (Galbraith and Sheetz, 1997) and others (Wakatsuki *et al.*, 2000) have facilitated measurement of cell properties such as cell elasticity, viscosity and cell contractile force became available. The model parameters that we use together with sources are summarized in Tables 1 and 2. According to published data a fibroblastic cell possesses significant elasticity. Its viscosity, on the other hand, is not very large. The large value of cell elasticity arises from the large density of actin in fibroblast cytoskeleton that is also enhanced by bundling. Large cell elasticity of fibroblast and small cell viscosity together with significant contractile force generation allow for fast compression of cytoskeleton when cell adhesions are released. Visually it is observed as 'jerky' fibroblast motion at the moment of adhesion release.

A variation of elastic and viscous properties over the cell length was observed in neutrophils (Yanai *et al.*, 1999). It was found that the protruding edge of a neutrophil has reduced stiffness and viscosity, that seems to be needed in order to form a protrusion. We do not account for this local event. However, we incorporate in our model that a cell may have spatial variation of elastic properties. Similar findings are made for fibroblasts (Nagayama *et al.*, 2001). Again, that

central region of the cell is found to be stiffer then the rest of the cell. The softening of the cell edge as well as nuclear region is observed when a stationary cell begins to move, however the cell maintains the relatively stiffer central part of the cytoskeleton. Cell elasticity is measured to be from 0.1×10^7 dyn cm^{-2} for the cell cortex (Bausch *et al.*, 1999), to 2.5×10^7 dyn cm^{-2} for the cell cytoskeleton (Wakatsuki *et al.*, 2000). We use values 1.0–5.0 Mdyn cm^{-2}. The fibroblast viscosity was reported to be small, with an approximate value of 2.0×10^3 dyn s cm^{-2} (Bausch *et al.*, 1999).

We estimated the parameter τ that is the contractile stress in the cell as a ratio of the cell contractile active force to the cell cross-sectional area $\tau_{\max} \approx f_0/S_{\text{cross}}$. The area is calculated as $S_{\text{cross}} = 1\ \mu\text{m} \times 30\ \mu\text{m} = 30\ \mu\text{m}^2$. Typical contractile force generated by a fibroblast is reported to be 500–1000 nN (Wakatsuki *et al.*, 2000). We use 1000 nN in our model. Then τ is estimated to be $\sim 0.3 \times 10^5$ dyn cm^{-2}.

We estimate the maximum value of drag coefficient as $\mu \sim \frac{\partial \tau}{\partial x} \cdot \frac{1}{v} = 0.03$ Mdyn cm$^{-2} \times 60$ s/0.2 μm ~ 10 Mdyn s cm^{-2} μm^{-1}/1 μm $= 10$ Mdyn s cm^{-4}. We use similar values in the model calculations.

We estimate the actin polymerization stress at the front of the model cell as $F_{\text{poly}} = 10^{-4}$ Mdyn cm^{-2}. We calculate this number by taking the number of actin at the front of $\sim 10^7$, single filament force of $F_{1\text{fil}} \sim 10^{-4}$ pN and cell lamellipodium cross-sectional area of $S_{\text{cross}} = 30\ \mu\text{m}^2$.

Appendix C: Analytical Solution

The analytical solution of the problem equations (2) and (3), for the case of small cytoskeletal viscosity $\mu(x) = 0$, can be written as follows

$$u(x,t) = \tilde{w}(x,t) + \frac{[\tau(f) - \tau(r)]}{\int_r^f dx\beta(x)} t + \int_r^x \frac{\tau(y) + f(y)}{E(y)} dy, \tag{C.1}$$

$$f(x) = \tau(r) + [\tau(f) - \tau(r)] \frac{\int_r^x dy\beta(y)}{\int_r^f dy\beta(y)}, \tag{C.2}$$

where $\tilde{w}(x,t)$ is a solution of the following problem

$$\frac{\partial}{\partial x}\left[E(x)\frac{\partial \tilde{w}}{\partial x}\right] = \mu_0(x)\frac{\partial \tilde{w}}{\partial t}, \tag{C.3}$$

$$E(x)\frac{\partial \tilde{w}}{\partial x}\bigg|_{r(t)} = 0, \qquad E(x)\frac{\partial \tilde{w}}{\partial x}\bigg|_{f(t)} = 0, \qquad \tilde{w}(x,0) = -\int_r^x \frac{\tau(y) + f(y)}{E(y)} dy. \tag{C.4}$$

In the limit of large times $t \to \infty$, the term $\tilde{w}(x, t \to \infty) \to$ constant, and the linear in time term dominates, so that

$$u(x,t) = \frac{\tau(f) - \tau(r)}{\int_r^f dx\beta(x)} t \tag{C.5}$$

and cell velocity is

$$v_{\text{cell}} = \frac{\tau(f) - \tau(r)}{\int_r^f dx\beta(x)}. \tag{C.6}$$

REFERENCES

Alberts, B., A. Johnson, J. Lewis, M. Raff, K. Roberts and P. Walter (2002). *Molecular Biology of the Cell*, 4th edn, New York and London: Garland.

Alt, W. and M. Dembo (1999). Epidemiology, cellular automata, and evolution—cytoplasm dynamics and cell motion: two-phase flow models. *Math. Biosci.* **156**, 207–1999.

Bausch, A., W. Moller and E. Sackmann (1999). Measurement of local viscoelasticity and forces in living cells by magnetic tweezers. *Biophys. J.* **76**, 573–579.

Bell, G. I. (1978). Models for the specific adhesion of cells to cells. *Science* **200**, 618–627.

Bershadsky, A. and B. Geiger (1999). Cytoskeleton-associated anchor and signal transduction proteins, in *Guidebook to the Extracellular Matrix, Anchor, and Adhesion Proteins*, Oxford: Oxford University Press, pp. 3–11.

Boal, D. (2002). *Mechanics of the Cell*, Cambridge: Cambridge University Press.

Bonner, J. T. (1998). A way of following individual cells in the migrating slugs of *Dictyostelium discoideum*. *PNAS USA* **95**, 9355–9359.

Bottino, D., A. Mogilner, T. Roberts, M. Stewart and G. Oster (2002). How nematode sperm crawl. *J. Cell Sci.* **115**, 367–384.

Bray, D. (2001). *Cell Movements: From Molecules to Motility*, New York: Garland Publishing.

Caille, N., O. Thoumine, Y. Tardy and J. Meister (2002). Contribution of the nucleus to the mechanical properties of endothelial cells. *J. Biomech.* **25**, 177–197.

Chew, T., W. Wolf and P. Gallagher (2002). A fluorescent resonant energy transfer-based biosensor reveals transient and regional myosin light chain kinase activation in lamella and cleavage furrows. *J. Cell Biol.* **156**, 543–553.

Chicurel, M. (2002). Cell migration research is on the move. *Science* **295**, 606–609.

Chrzanowska-Wodnicka, M. and K. Burridge (1996). Rho-stimulated contractility drives the formation of stress fiber and focal adhesions. *J. Cell Biol.* **133**, 1403–1415.

Cox, E. and A. Huttenlocher (1998). Regulation of integrin-mediated adhesion during cell migration. *Microsc. Res. Tech.* **43**, 412–419.

Defilippi, P., C. Olivo and M. Venturino (1999). Actin cytoskeleton organization in response to integrin-mediated adhesion. *Microsc. Res. Tech.* **47**, 67–78.

Dembo, M. and Y. L. Wang (1999). Stresses at the cell-to-substrate interface during locomotion of fibroblasts. *Biophys. J.* **76**, 2307–2316.

DiMilla, P. A., K. Barbee and D. A. Lauffenburger (1991). Mathematical model for the effects of adhesion and mechanics on cell migration speed. *Biophys. J.* **60**, 15–37.

Dong, C. and R. Skalak (1992). Leukocyte deformability: finite element modeling of large viscoelastic deformation. *J. Theor. Biol.* **158**, 173–193.

Dumontier, M., P. Hocht, U. Mintert and J. Faix (2000). Rac1 GTPases control filopodia formation, cell motility, endocytosis, cytokinesis and development in *Dictyostelium*. *J. Cell Sci.* **113**, 2253–2265.

Evans, E. and A. Yeung (1989). Apparent viscosity and cortical tension of blood granulocytes determined by micropipet aspiration. *Biophys. J.* **56**, 151–160.

Felder, S. and E. L. Elson (1990). Mechanics of fibroblast locomotion: quantitative analysis of forces and motions at the leading lamellas of fibroblasts. *J. Cell Biol.* **111**, 2513–2526.

Felsenfeld, D. P., P. L. Schwartzberg, A. Venegas, R. Tse and M. P. Sheetz (1999). Selective regulation of integrin–cytoskeleton interactions by the tyrosine kinase Src. *Nature Cell Biol.* **1**, 200–206.

Feneberg, W. and M. Westphal (2001). *Dictyostelium* cells' cytoplasm as an active viscoplastic body. *Euro. Biophys. J.* **30**, 284–294.

Galbraith, C. G. and M. P. Sheetz (1997). A micromachined device provides a new bend on fibroblast traction forces. *PNAS USA* **94**, 9114–9118.

Gliksman, N. R., G. Santoyo, K. D. Novak and M. A. Titus (2001). Myosin I phosphorylation is increased by chemotactic stimulation. *J. Biol. Chem.* **276**, 5235–5239.

Heidemann, S. R., S. Kaech, R. E. Buxbaum and A. Matus (1999). Direct observations of the mechanical behaviors of the cytoskeleton in living fibroblasts. *J. Cell Biol.* **145**, 109–122.

Hollenbeck, P. (2001). Cytoskeleton: microtubules get the signal. *Curr. Biol.* **11**, R820–R823.

Howe, A., A. Aplin and A. Alahari (1998). Integrin signaling and cell growth control. *Curr. Opin. Cell Biol.* **10**, 220–231.

Janmey, P. (1991). Mechanical properties of cytoskeletal polymers. *Curr. Opin. Cell Biol.* **2**, 4–11.

Janmey, P. (1998). The cytoskeleton and cell signalling: component localization and mechanical coupling. *Physiol. Rev.* **78**, 763–781.

Kaverina, I., O. Krylyshkina and J. V. Small (2002). Regulation of substrate adhesion dynamics during cell motility. *Int. J. Biochem. Cell Biol.* **34**, 746–761.

Landau, L. and E. Lifshits (1965). *Theory of Elasticity*, Moscow: Science.

Lauffenburger, D. A. (1989). A simple model for the effects of receptor-mediated cell-substratum adhesion on cell migration. *Chem. Eng. Sci.* **44**, 1903–1914.

Lauffenburger, D. and A. Horwitz (1996). Cell migration: a physically integrated molecular process. *Cell* **84**, 359–369.

Lo, C. M., H. B. Wang, M. Dembo and Y. L. Wang (2000). Cell movement is guided by the rigidity of the substrate. *Biophys. J.* **79**, 144–152.

MacKintosh, F. C. (1998). Theoretical models of viscoelasticity of actin solutions and the actin cortex. *Biol. Bull.* **194**, 351–353.

Maheshwari, G., G. Brown, D. A. Lauffenburger, A. Wells and L. G. Griffith (2000). Cell adhesion and motility depend on nanoscale RGD clustering. *J. Cell Sci.* **10**, 1677–1686.

Martin, K., J. Slack and S. Boerner (2002). Integrin connections map: to infinity and beyond. *Science* **296**, 1652–1653.

Mitchison, T. J. and L. P. Cramer (1996). Actin-based cell motility and cell locomotion. *Cell* **84**, 371–379.

Mogilner, A. and L. Edelstein-Keshet (2002). Regulation of actin dynamics in rapidly moving cells: a quantitative analysis. *Biophys. J.* **83**, 1237–1258.

Mogilner, A. and D. W. Verzi (2003). A simple 1-D physical model for the crawling nematode sperm cell. *J. Stat. Phys.* **110**, 1169–1189.

Mogilner, A., E. Marland and D. Bottino (2000). A minimal model of locomotion applied to the steady gliding movement of fish keratocyte cells, in *Mathematical Models for Biological Pattern Formation*, New York: Springer, pp. 269–294.

Munevar, S., Y. L. Wang and M. Dembo (2001a). Distinct roles of frontal and rear cell–substrate adhesions in fibroblast migration. *Mol. Biol. Cell* **12**, 3947–3954.

Munevar, S., Y. Wang and M. Dembo (2001b). Traction force microscopy of migrating normal and H-ras transformed 3T3 fibroblasts. *Biophys. J.* **80**, 1744–1757.

Nagayama, M., H. Haga and K. Kawabata (2001). Drastic change of local stiffness distribution correlating to cell migration in living fibroblasts. *Cell Motil. Cytoskeleton* **50**, 173–179.

Palecek, S. P., C. E. Schmidt, D. A. Lauffenburger and A. F. Horwitz (1996). Integrin dynamics on the tail region of migrating fibroblasts. *J. Cell Sci.* **5**, 941–952.

Palecek, S. P., J. C. Loftus, M. H. Ginsberg, D. A. Lauffenburger and A. F. Horwitz (1997). Integrin–ligand binding properties govern cell migration speed through cell–substratum adhesiveness. *Nature* **385**, 537–540.

Palsson, E. and H. G. Othmer (2000). A model for individual and collective cell movement in Dictyostelium discoideum. *PNAS USA* **97**, 10448–10453.

Ragsdale, G. K., J. Phelps and K. Luby-Phelps (1997). Viscoelastic response of fibroblasts to tension transmitted through adherens junctions. *Biophys. J.* **73**, 2798–2808.

Samarsky, A. A. (1983). *Theory of Finite-Difference Methods*, Moscow: Science.

Schimd-Schönbein, G., T. Kosawada, R. Skalak and S. Chien (1995). Membrane model of endothelial cells and leukocytes. A proposal for the origin of a cortical stress. *J. Biomech. Eng.* **117**, 171–178.

Sheetz, M. P., D. Felsenfeld, C. G. Galbraith and D. Choquet (1999). Cell migration as a five-step cycle. *Biochem. Soc. Symp.* **65**, 233–243.

Skalak, R., C. Dong and C. Zhu (1990). Passive deformations and active motions of leukocytes. *J. Biomech. Eng.* **112**, 295–302.

Small, J. V. (1989). Microfilament-based motility in non-muscle cells. *Curr. Opin. Cell Biol.* **1**, 75–79.

Sod, G. (1985). *Numerical Methods for Fluid Dynamics: Initial and Initial Boundary-value Problems*, New York: Cambridge Univeristy Press.

Soll, D. R. (1995). The use of computers in understanding how animal cells crawl, in *International Review of Cytology*, vol. 163, K. W. Jeon and J. Jarvik (Eds), Acdemic Press, pp. 43–104.

Theriot, J. and T. Mitchison (1991). Actin microfilament dynamics in locomoting cells. *Nature* **352**, 107–108.

Verkhovsky, A. B., T. M. Svitkina and G. G. Borisy (1999). Self-polarization and directional motility of cytoplasm. *Curr. Biol.* **9**, 11–20.

Wakatsuki, T., M. S. Kolodney, G. I. Zahalak and E. L. Elson (2000). Cell mechanics studied by a reconstituted model tissue. *Biophys. J.* **79**, 2353–2368.

Wang, H. B., M. Dembo, S. K. Hanks and Y. Wang (2001). Focal adhesion kinase is involved in mechanosensing during fibroblast migration. *PNAS USA* **98**, 11295–11300.

Wood, W. and P. Martin (2002). Structures in focus-filopodia. *Int. J. Biochem. Cell Biol.* **34**, 726–730.

Xu, J., Y. Tseng and D. Wirtz (2000). Strain hardening of actin filament networks. *J. Biol. Chem.* **46**, 35886–35892.

Yanai, M., J. P. Butler, T. Suzuki, A. Kanda, M. Kurachi, H. Tashiro and H. Sasaki (1999). Intracellular elasticity and viscosity in the body, leading, and trailing regions of locomoting neutrophils. *Am. J. Physiol.* **277**, C432–C440.

Yeung, A. and E. Evans (1989). Cortical shell-liquid core model for passive flow of liquid-like spherical cells into micropipets. *Biophys. J.* **56**, 139–149.

Zamir, E. and B. Geiger (2001). Molecular complexity and dynamics of cell-matrix adhesions. *J. Cell Sci.* **20**, 3583–3590.

Received 3 July 2003 and accepted 28 August 2003